Electron impact vibrational excitation of carbon monoxide in the upper atmospheres of Mars and Venus

L. Campbell,[1] M. Allan,[2] and M. J. Brunger[1,3]

Received 17 May 2011; revised 15 June 2011; accepted 28 June 2011; published 24 September 2011.

[1] Infrared emission from CO in the upper atmospheres of Mars, Venus and several other planets is a subject of current theoretical and experimental interest. Electron impact excitation makes a contribution that has not been included in previous studies. Given this, and recent new measurements of absolute cross sections for low-energy electron impact excitation of the vibrational levels of the ground state of CO, results from calculations are presented showing the contribution of electron impact relative to emissions by other mechanisms. It is demonstrated that emissions due to the impact of thermal, photo- and auroral electrons are generally small compared to sunlight-driven (fluorescence and photolysis) emissions, but with some exceptions. It is also shown that thermal-electron emissions may dominate over other processes at nighttime at Mars and that auroral emissions certainly do so. While measurements and other calculations do not appear to be available for Venus, the volume emission rates presented should be valuable in planning such measurements.

Citation: Campbell, L., M. Allan, and M. J. Brunger (2011), Electron impact vibrational excitation of carbon monoxide in the upper atmospheres of Mars and Venus, *J. Geophys. Res.*, *116*, A09321, doi:10.1029/2011JA016848.

1. Introduction

[2] Observations and modeling of carbon monoxide (CO) infrared emissions from the upper atmospheres of Venus, Mars and Earth are currently being conducted [*Gilli et al.*, 2011]. CO infrared emissions have also been observed from Jupiter [*Brooke et al.*, 1996], Titan [*Baines et al.*, 2006], Uranus [*Encrenaz et al.*, 2004] and Neptune [*Fletcher et al.*, 2010]. These emissions are taken to be from molecules excited by solar fluorescence and photolysis, or collisional processes, without mention of the possibility of electron impact excitation. Solar extreme ultraviolet radiation and energetic charged particles produce ionization in planetary atmospheres [*Nagy and Cravens*, 2002] and suprathermal electron distributions (photoelectrons or auroral electrons). Further collisions produce a background of thermal electrons. Given that relatively recent measurements of electron vibrational excitation of CO have been made [*Poparić et al.*, 2006; *Allan*, 2010], it is timely to compare the emissions expected from electron-impact excitation with those from the other processes.

[3] Carbon dioxide (CO_2) and CO are the major molecular gases in the upper atmosphere of Venus with CO predominant above 150 km [*Kasprzak et al.*, 1993]. In the upper atmosphere of Mars, CO_2 is predominant, followed by N_2, with CO rising in proportion to CO_2 with altitude and having a density of ~10% of that of CO_2 at 180 km [*Nier and McElroy*, 1977]. Calculations of electron cooling rates showed that vibrational excitation of CO was more significant than that of CO_2 above ~168 km for Venus and above ~300 km for Mars [*Campbell and Brunger*, 2008]. Due to larger cross sections at lower energies and a lower appearance energy, CO_2 was predicted to produce much greater cooling rates than CO at the low electron temperatures at lower altitudes [*Campbell et al.*, 2008], but it is still worthwhile to predict CO emissions at lower altitudes as a possible point of comparison between models and measurements.

[4] In section 2 the two most recent sets of absolute measurements of electron-impact excitation of the vibrational levels of CO are presented and compared. The differences are illustrated by updating results from previous calculations of electron cooling rates in the atmospheres of Mars and Venus. In section 3 the methods and parameters for our more detailed calculations are presented, then in section 4 the calculated emissions due to electron impact are compared with values for other processes, leading to the conclusions in section 5.

2. Electron-Impact Excitation Cross Sections

[5] Relative integral cross sections for vibrational excitation of CO [*Allan*, 1989] could be put on an absolute scale by reference to an absolute measurement at 1.91 eV [*Gibson et al.*, 1996]. This was about 35% higher than earlier measurements. More recent measurements by *Poparić et al.*

[1]ARC Centre for Antimatter-Matter Studies, School of Chemical and Physical Sciences, Flinders University, Adelaide, South Australia, Australia.
[2]Department of Chemistry, University of Fribourg, Fribourg, Switzerland.
[3]Also at Institute of Mathematical Sciences, University of Malaya, Kuala Lumpur, Malaysia.

Copyright 2011 by the American Geophysical Union.
0148-0227/11/2011JA016848

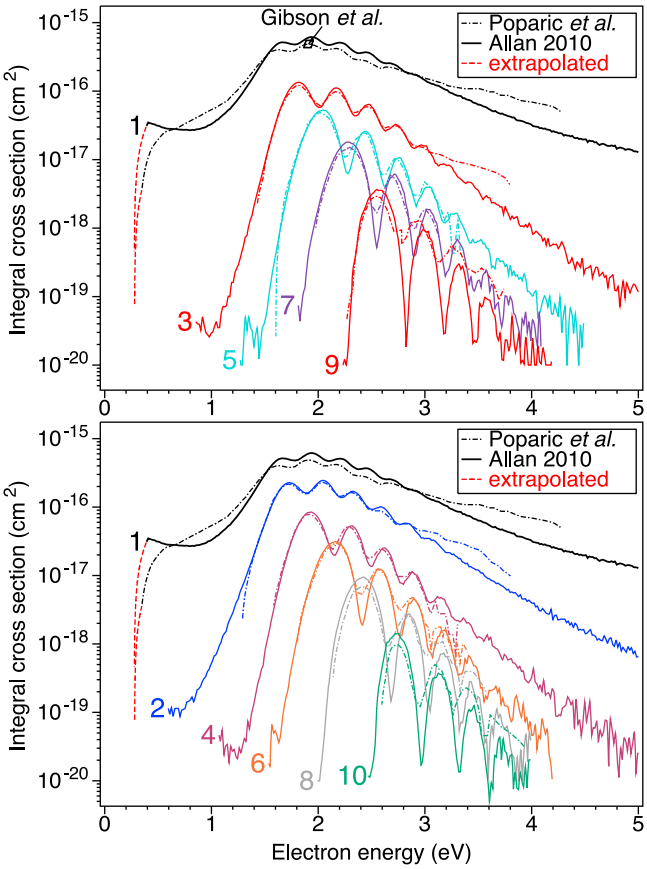

Figure 1. Integral cross sections of *Allan* [2010] (solid lines) and *Poparić et al.* [2006] (dot-dashed lines) for electron impact excitation of vibrational levels $0 \rightarrow \nu' = 1$, 2,.., 10 of CO. Extrapolation (dashed line) is applied at the low-energy end for $0 \rightarrow \nu' = 1$. The value of *Gibson et al.* [1996] at 1.91 eV is shown.

[2006] were scaled to the same absolute value. Hence there was a need for independent absolute measurements, which have recently been made by *Allan* [2010]. These most recent independent sets of measurements are compared in Figure 1, for excitation of levels $\nu' = 1 - 10$ of CO. Dashed lines indicate extrapolation of both sets of measurements at the low-energy limit for $\nu' = 1$. A comparison shows that there is good agreement between the measurements of *Poparić et al.* [2006] and of *Allan* [2010] for $\nu' > 1$ (except that Allan's values extend to lower energies), but that there are significant differences for the $\nu' = 1$ excitation in terms of both shape and maximum value.

[6] The consequences of the new measurements for atmospheric simulations are shown for calculations of electron cooling rates in the atmospheres of Mars and Venus, in Figures 2 and 3 respectively. These are updates of previous work [*Campbell and Brunger*, 2008], in which calculations based on the scaled measurements of *Allan* [1989], labeled "previous", were compared with calculations based on measurements by *Poparić et al.* [2006], labeled "Poparic." The new calculations based on the absolute measurements of *Allan* [2010] are labeled "current".

[7] The electron cooling rate, as introduced for CO_2 in the Martian atmosphere by *Morrison and Greene* [1978], is the rate at which electrons lose energy via impact excitation of molecules. *Campbell and Brunger* [2008] used the formulation of *Pavlov* [1998] to calculate electron energy transfer rates, which, when multiplied by the density, give the electron cooling rates. It can be seen in Figures 2 and 3 for the $(0 \rightarrow 1)$ excitation that there is not much difference between the cooling rates using the scaled values of *Allan* [1989] and the more recent cross sections of *Allan* [2010]. (This seems to be in conflict with the larger maximum value of the cross section in the more recent measurements. However, due to the much higher electron fluxes at lower energies in the Maxwell-Boltzmann distribution, the much smaller reduction in cross sections around 1 eV can lead to a reduction in the cooling rate that is as large as the increase produced by the higher cross sections around 2 eV.) The conclusion here is the same as that in the earlier work of *Campbell and Brunger* [2008], that the cooling rates at low temperatures (at altitudes 100–200 km for Mars and 140–160 km for Venus) are significantly larger using the cross sections of *Allan* [1989, 2010], relative to those using the cross sections of *Poparić et al.* [2006], as expected due the extension of Allan's measurements to lower energies. The cooling rates for $\nu' = 2 - 10$ are larger for the absolute measurements of *Allan* [2010] in the altitude ranges 160–170 km at Mars and 140–170 km at Venus, again due to the

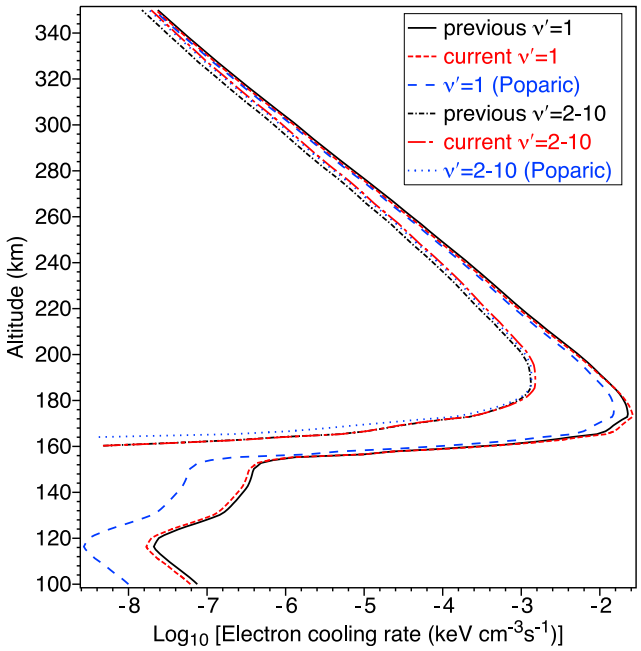

Figure 2. Electron cooling rates (horizontal axis) as a function of altitude in the atmosphere of Mars. Values for the $\nu' = 1$ excitation are shown for the previous (solid curve) and current (short dashed curve) calculations using the cross sections of *Allan* [1989] and *Allan* [2010], respectively, and for calculations using the cross sections of *Poparić et al.* [2006] (long dashed curve). Similarly the rates for the sum of the $\nu' = 2$, 3,.., 10 excitations are shown for the previous (dot-short-dashed curve), current (dot-long-dashed curve) and *Poparić et al.* [2006] (dotted curve) cases.

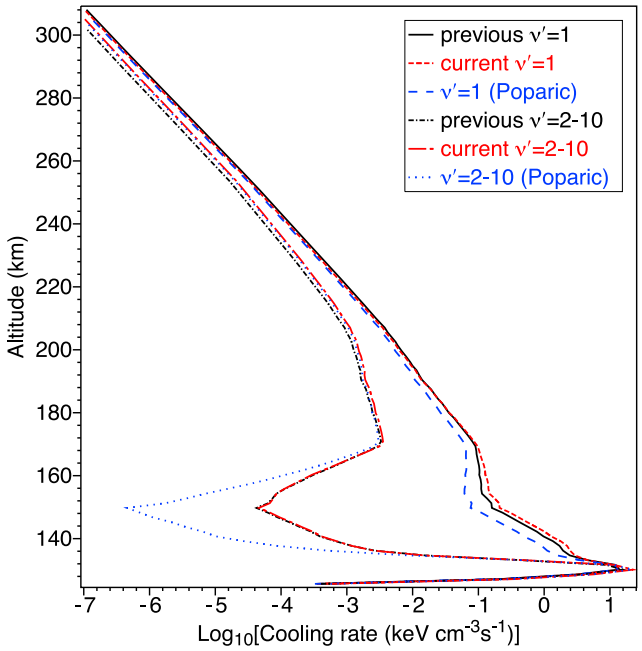

Figure 3. Electron cooling rates (horizontal axis) as a function of altitude in the atmosphere of Venus. Values for the $\nu' = 1$ excitation are shown for the previous (solid curve) and current (short dashed curve) calculations using the cross sections of *Allan* [1989] and *Allan* [2010], respectively, and for calculations using the cross sections of *Poparić et al.* [2006] (long dashed curve). Similarly the rates for the sum of the $\nu' = 2$, 3,.., 10 excitations are shown for the previous (dot-short-dashed curve), current (dot-long-dashed curve) and *Poparić et al.* [2006] (dotted curve) cases.

extension of the measurements of *Allan* [2010] to lower energies compared to the measurements of *Poparić et al.* [2006].

3. Methods of Calculation

[8] The method of *Pavlov* [1998] used in section 2 applies only to excitation produced by electrons with a Maxwell-Boltzmann distribution of energies, often referred to as thermal electrons, characterized by an electron temperature. To allow for suprathermal electrons in planetary atmospheres, such as auroral electrons and photoelectrons, calculations require a flux spectrum (i.e., flux of electrons as a function of electron energy). The excitation rate is then determined by multiplying the flux by the integral cross section at each energy and summing over all energies.

[9] For the atmosphere of Venus measurements of the nighttime suprathermal flux spectrum are given by *Spenner et al.* [1996] for various heights at and above 168 km, while a calculated spectrum at 139 km is given by *Gérard et al.* [2008]. The spectra of Spenner et al. are subject to considerable variation which obscures the variation with height, and have no values below 8 eV. The absolute values of the flux of Gérard et al. are substantially greater than those of Spenner et al., despite being for a lower altitude. This may be explained by the values of Gérard et al. being for solar maximum and those of Spenner et al. being for moderate solar activity, but in both papers it is reported that there is not much variation with solar activity. As this work involves an emulation of some calculations by *Gronoff et al.* [2008] that use the fluxes of Spenner et al., the procedure here is to use the values of Spenner et al. as a base and those of Gérard et al. for the shape of the spectrum at low energies, to determine an auroral spectrum as a function of altitude. The steps in the procedure are illustrated in Figure 4. Given the variability and contradictions in the available data, this procedure cannot be considered to be totally rigorous, but rather is intended to produce flux spectra that are as consistent as practical with the two sources.

[10] *Spenner et al.* [1996] present a number of unlabeled flux spectra. The heights for individual spectra were deduced for this work by reference to their Figure 2. To cope with the variability of the spectra, two "base" spectra are calculated, for 168 km by taking the average of spectra at 182 and 195 km, and for 600 km by taking the average of values for 259, 425, 429 and 592 km. These combinations were selected because they produced average spectra of similar shape, facilitating an extrapolation to lower altitudes by the procedure described below.

[11] It is assumed that, given a flux spectrum $F(h, E)$ at height h and energy E, the spectrum at $F(h - \Delta h, E)$ is given by

$$F(h - \Delta h, E) = F(h, E) - k(E)D(h) \quad (1)$$

where $k(E)$ is a constant for energy E and $D(h)$ is the sum of the densities of O, CO and N_2 at height h (km); $k(E)$ is found

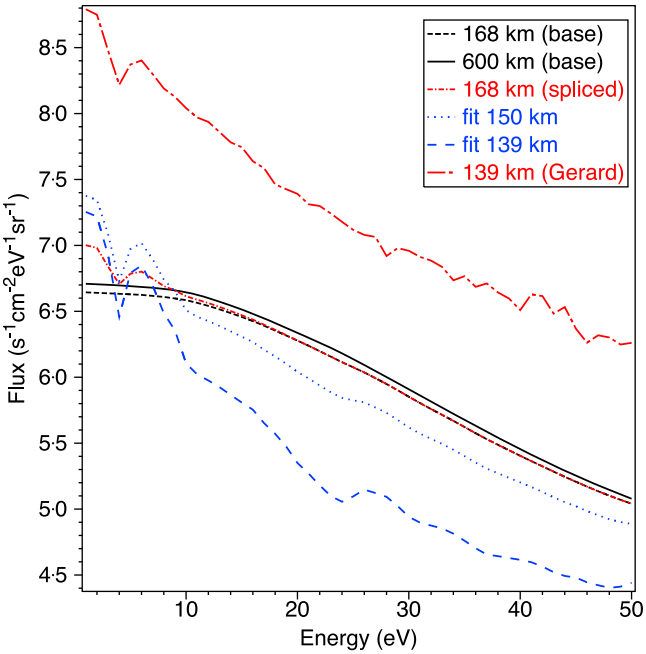

Figure 4. Spectra of auroral electrons at night in the atmosphere of Venus. Two base spectra at 168 km (short dashed curve) and 600 km (solid curve) are deduced from the profiles of *Spenner et al.* [1996]. The shape at low-energy of a spectrum at 139 km of *Gérard et al.* [2008] (dot-long-dashed curve) is spliced onto the base spectrum at 168 km (dot-short-dashed curve). Calculated spectra extrapolated from these are shown for 139 km (long dashed curve) and 150 km (dotted curve).

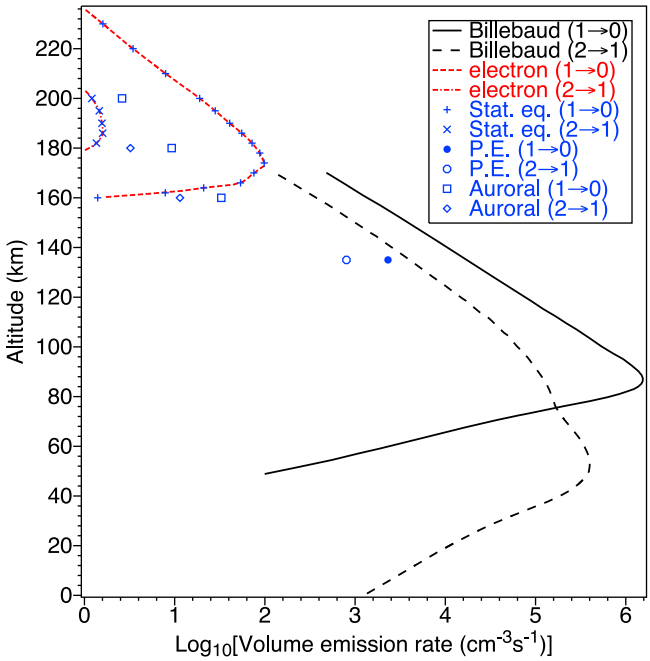

Figure 5. Volume emission rates (horizontal axis) as a function of altitude in the atmosphere of Mars, as calculated by *Billebaud et al.* [1991] for (1 → 0) (solid curve) and (2 → 1) (long dashed curve) and in the current calculation for (1 → 0) (short dashed curve) and (2 → 1) (dot-dashed curve). Symbols show the current results with collisional quenching included for (1 → 0) (plus) and (2 → 1) (cross), for photoelectrons [*Shematovich et al.*, 2008] for (1 → 0) (bullet) and (2 → 1) (circle) and for auroral excitation [*Leblanc et al.*, 2006] of (1 → 0) (square) and (2 → 1) (diamond).

iteratively by calculating values of $F(168, E)$ from $F(600, E)$ for different values of $k(E)$. (In each iteration, equation (1) is applied at intervals of $\Delta h = 0.01$ km, from 599.99 km down to 168 km.) Equation (1) can then be applied in the same way, using the now-determined constants $k(E)$, to calculate base spectra at all altitudes below 168 km. In applying this calculation it is found that the maximum rate of flux loss occurs at 145 km, close to the value of 139 km found by *Gérard et al.* [2008], providing some validation that this is an acceptable procedure.

[12] The measured spectrum of *Spenner et al.* [1996] at 168 km rises rapidly toward the low-energy cut-off at 8 eV. It is assumed that this corresponds to the low-energy peaks in the spectrum of *Gérard et al.* [2008]. As the flux spectra at 182 and 195 km do not have this rise, an average of the values at 168, 182 and 195 km is taken as a best estimate of the low-energy (8–10 eV) flux at 168 km. By matching the slope for 8–10 eV in this average spectrum to the same part of the spectrum of Gérard et al., a scaled portion of the spectrum of Gérard et al. for 1–8 eV can be added to the base 168-km spectrum. A linear interpolation is then applied between 10 and 20 eV to produce a "spliced" 168-km spectrum, as shown in Figure 4. On the assumption that the flux of low-energy electrons is proportional to the loss rate of electrons at higher energy (as the low-energy electrons are produced in the ionization processes in which the higher-energy electrons are being lost), the low-energy section added at 168 km is added at all other heights, but scaled to the loss rate in the base spectrum at each height. Thus the relative contribution at low energies is larger at lower heights where the base flux is being reduced more quickly, as seen in Figure 4 for the calculated spectra at 150 km and 139 km.

[13] A second limitation of the method used in section 2 is that only excitation/cooling is calculated. Other processes, such as the production of vibrationally excited CO by the radiative decay of excited electronic states to $\nu'' > 0$ levels of the ground state, the stepwise decay of vibrationally excited levels of the ground state (e.g., (2 → 1) followed by (1 → 0) transitions) and quenching (where excited molecules lose energy in collisions rather than radiating) are not included. This mix of processes can however be handled by a statistical-equilibrium calculation [*Cartwright et al.*, 2000; *Campbell et al.*, 2006, 2007, 2010]. In this the continuity equations are solved (i.e., adjusting the population to set gain equal to loss) for each level of each excited state, with the process applied repetitively until all population densities become stable.

[14] CO_2 is the only quenching molecule considered in this study, as it is the dominant species at altitudes where densities are high enough for quenching to be significant. Rates for the reaction:

$$CO(\nu = 1) + CO_2(000) \rightarrow CO(\nu = 0) + CO_2(001) \qquad (2)$$

were given by *Starr and Hancock* [1975]. These can be approximately represented by

$$Q(T) = 1.942 \times 10^{-21} T^3 - 4.517 \times 10^{-19} T^2 + 2.639 \times 10^{-16} T - 1.783 \times 10^{-14} \ \mathrm{cm^3 s^{-1} molecule^{-1}}, \qquad (3)$$

where $Q(T)$ is the quenching rate at temperature T (K). For quenching of excited electronic states, rates for quenching of $CO(a\ ^3\Pi)$ by CO_2 from *Lawrence* [1971] were used.

4. Comparison With Other Processes

[15] For direct comparison with measurements and calculations by other researchers, results are henceforth presented as "volume emission rates," i.e., photons/cm^3/s. (In the absence of collisional quenching, these are equal to the cooling rates divided by the energies of the emitted photons.)

[16] In Figure 5 calculations of daytime CO emissions (1 → 0) and (2 → 1) by *Billebaud et al.* [1991] are plotted as a function of height in the Martian atmosphere. The excitation mechanisms considered were solar infrared excitation of CO and production of excited CO by the photolysis of CO_2. Current calculations using the formulation of *Pavlov* [1998] of the emissions due to impact excitation by thermal electrons (using electron densities, electron temperatures and neutral densities as described by *Campbell and Brunger* [2008]) are shown by dashed lines. It is seen that the emissions due to thermal electrons are insignificant below ~168 km, but that the (1 → 0) emissions are of similar magnitude to the other production mechanisms (extrapolating these visually) at higher altitudes. The volume-emission-rate ratio for (2 → 1)/(1 → 0) appears to be substantially less for the electron-excitation case, raising the possibility that

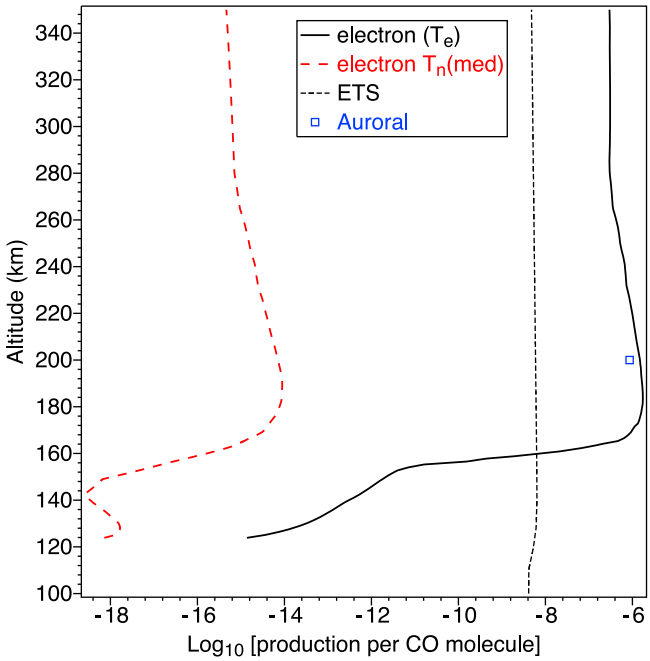

Figure 6. Production rate of CO photons per molecule (horizontal axis) as calculated by *López-Valverde and López-Puertas* [1994] for "emission to space" (short dashed line) and for impact by thermal electrons with characteristic temperatures equal to the nighttime neutral temperature for medium solar activity [*González-Galindo et al.*, 2005] (long dashed line) and equal to the daytime electron temperature [*Choi et al.*, 1998] (solid line). The value due to auroral excitation [*Leblanc et al.*, 2006] is shown at 200 km (square).

emissions due to the two different mechanisms can be distinguished by measuring this ratio. Emission rates calculated using the full statistical-equilibrium calculation have values indistinguishable from the *Pavlov* [1998] method, showing that quenching is negligible in this instance. (This agreement also provides a self-consistency check on the accuracy of the two different methods of calculation, as the statistical-equilibrium calculation is coupled with an electron-flux spectrum for the thermal electrons. The flux spectrum is necessary for the following calculations with suprathermal (i.e., non-Maxwell-Boltzmann) electrons.)

[17] The emissions due to impact by photoelectrons at 135 km are shown, based on the photoelectron flux spectrum calculated by *Shematovich et al.* [2008]. These are about 10% of the other production rates and hence insignificant for this height. (As it is shown below that photoelectron excitation exceeds that by thermal electrons at 250 km in the atmosphere of Venus, it is plausible that the same applies here, in which case photoelectron excitation would be the dominant excitation mechanism above ~168 km.) Auroral emissions, calculated using an electron flux spectrum measured by "MAX/ASPERA-3" [*Leblanc et al.*, 2006], are shown for heights above 160 km (based on the assumption that there is no significant reduction in flux above 160 km). Again these are not significant compared to the solar-driven emissions.

[18] For Mars at night, the production rate of photons per CO molecule was calculated by *López-Valverde and López-Puertas* [1994] by considering both collisional processes and radiative transfer. Their values for "emission to space" are shown in Figure 6 as the curve labeled "ETS". Current calculations for emissions due to excitation by thermal electrons are shown for two cases. The curve labeled "electron T_n(med)" is calculated with an electron temperature equal to the neutral temperature at night for medium solar activity, as calculated by *González-Galindo et al.* [2005]. The curve labeled "electron (T_e)" is calculated using the daytime electron temperature calculated by *Choi et al.* [1998]. *Lillis et al.* [2009] argue that it is appropriate to assume that the nighttime electron temperature can be approximated by the daytime electron temperature rather than the nighttime neutral temperature. So CO emissions due to thermal-electron impact should be dominant above ~160 km if this assumption is correct.

[19] The value of the production rate produced by the auroral flux is shown at 200 km. (This will be the same value at all heights above where the flux is significantly reduced by absorption.) It is almost equal to the maximum rate for the thermal electrons, and significantly larger than the processes modeled by *López-Valverde and López-Puertas* [1994].

[20] In Figure 7 current calculations of Cameron ($a\ ^3\Pi \rightarrow X\ ^1\Sigma^+$) and Fourth Positive band ($A\ ^1\Pi \rightarrow X\ ^1\Sigma^+$) emissions are compared with values calculated by *Gronoff et al.* [2008], for auroral emissions in the atmosphere of Venus. Obviously in this case the atmospheric parameters given by Gronoff et al. were used rather than those from the earlier work [*Campbell and Brunger*, 2008]. The electron-impact cross sections of *Furlong and Newell* [1996] were used to calculate excitation rates for $a\ ^3\Pi$ and those of *Kato et al.* [2007] for $A\ ^1\Pi$. The statistical-equilibrium calculation was used to allow the inclusion of quenching and $a'\ ^3\Sigma^+ \rightarrow a\ ^3\Pi$ transitions.

[21] For the Cameron bands the current calculation gives volume emission rates about 2.5 times those of *Gronoff et al.* [2008] (above 180 km). To investigate this discrepancy, the calculation was repeated using the cross sections of *Ajello* [1971], as used by Gronoff et al. In this test the predicted Cameron band emissions are very close to those of Gronoff et al. This agreement suggests that the current implementation (developed in section 3) of the flux spectra of *Spenner et al.* [1996] is very similar to that of Gronoff et al. and that the current calculations are correctly implemented.

[22] A similar comparison for the Fourth Positive band emissions is ambiguous. The current values (based on recent electron-impact excitation cross sections of *Kato et al.* [2007]) are about 10 times larger than given by *Gronoff et al.* [2008] and are only slightly smaller when calculated with the cross sections of *Beegle et al.* [1999], cited as the source by Gronoff et al. When the current calculations were performed using cross sections from Table 3 of Beegle et al. (i.e., for excitation of only the $A\ ^1\Pi(\nu' = 0)$ level) the predicted emissions are very close to those of Gronoff et al. (above 180 km), so the explanation for the discrepancy may be that Gronoff et al. presented results for excitation to the $A\ ^1\Pi(\nu' = 0)$ level only. (Note that while different values of Franck Condon factors may have been employed here relative to those used by Gronoff et al., this does not change the volume emission rates when applying the cross sections of Beegle et al. in the absence of quenching, and is

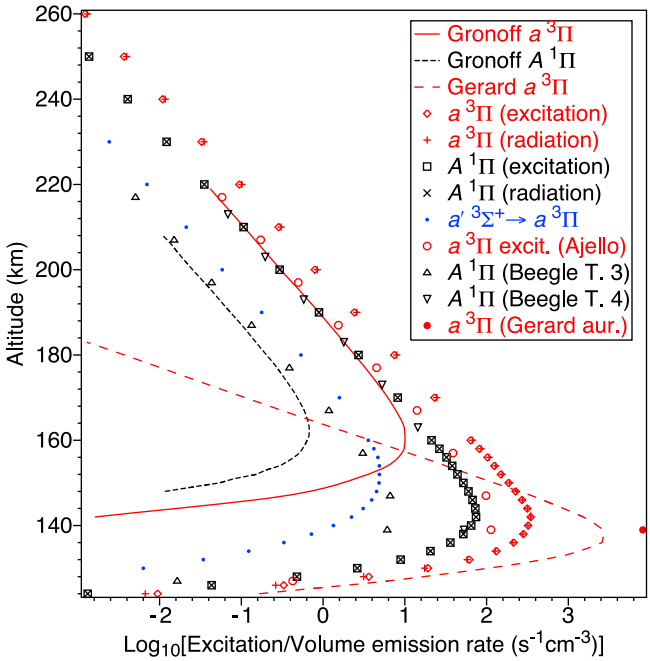

Figure 7. Excited state CO excitation rates and volume emission rates due to auroral excitation in the atmosphere of Venus: calculations of the Cameron bands by *Gronoff et al.* [2008] (solid curve) and by *Gérard et al.* [2008] (long dashed curve) and of the Fourth Positive bands by *Gronoff et al.* [2008] (short dashed curve); current calculations of excitation and emission rates for the Cameron bands (diamonds and pluses), Fourth Positive bands (squares and crosses) and Asundi bands (dots); current calculations for the Cameron bands using the cross sections of *Ajello* [1971] (circles), Fourth Positive bands using cross sections from Table 4 of *Beegle et al.* [1999] (inverted triangles) and the $A\ ^1\Pi(v' = 1)$ level using Table 3 of Beegle et al. (triangles); current calculations using the electron flux spectrum of *Gérard et al.* [2008] at 139 km (bullet).

not relevant when using the cross sections of Kato et al. as these are measured for individual vibrational levels.)

[23] Below 180 km the current calculation gives values significantly higher than those of *Gronoff et al.* [2008], with a peak at 142 km rather than 160 km. This is consistent with the calculation of the Cameron bands by *Gérard et al.* [2008] (long dashed curve) which has peak emissions at 139 km. In Figure 7 the absolute intensity is about 10 times less than that of Gérard et al., rather than the factor of 100 that might be expected by comparison of the flux spectra in Figure 4. To investigate this the current calculation was performed using the flux spectrum of Gérard et al. at 139 km and the cross sections of *Ajello* [1971] (note that it is not clear which cross sections were used by Gérard et al.), giving a value about 3.5 times as large as in the curve published by Gérard *at al.* The source of this discrepancy is unknown, but the calculated value is nearly 100 times the current calculation with the cross sections of Ajello et al. (circle), and so is consistent with the flux values in Figure 4. Considering the large differences in the altitude profiles for the Cameron emissions between those of *Gronoff et al.* [2008] and *Gérard et al.* [2008], the current model (of which the altitude profile depends only on the measurements of *Spenner et al.* [1996] and equation (1)) appears to be reasonable, in that it gives values for Cameron-band emissions in agreement with those of *Gronoff et al.* [2008] above 180 km and independently finds nearly the same altitude of maximum emissions as those of *Gérard et al.* [2008].

[24] The excitation and radiation rates are shown for the current calculations of both the Cameron and Fourth Positive bands. Significant quenching (indicated by the radiation rate being less than the excitation rate) is only apparent for the Cameron bands below ~138 km.

[25] It was suggested [*Slanger et al.*, 2008] that transitions from the $a'\ ^3\Sigma^+$, $d\ ^3\Delta$ and $e\ ^3\Sigma^-$ states to $a\ ^3\Pi$ might be substantial in the atmospheres of Mars and Venus. Electron-impact cross sections are available for the $a'\ ^3\Sigma^+$ state [*Brunger et al.*, 2003], allowing the Asundi band ($a'\ ^3\Sigma^+ \rightarrow A\ ^3\Pi$) emissions to be included in Figure 7. These are small compared to the Cameron band emissions, so their contribution to the Cameron bands (shown by the excess of radiation over excitation for $a\ ^3\Pi$) is also small.

[26] In Figure 8 various calculations of CO ($1 \rightarrow 0$) emissions are compared with the calculations of *Crovisier et al.* [2006] for daytime emissions in the atmosphere of Venus due to fluorescence and photolysis. The method of *Pavlov* [1998] was used to calculate the ($1 \rightarrow 0$) volume

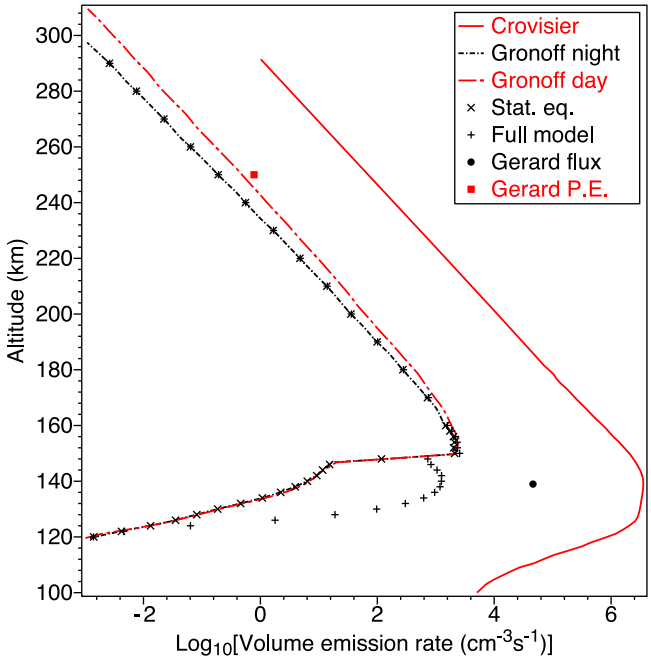

Figure 8. Comparison of electron-driven CO ($1 \rightarrow 0$) volume emission rates to calculations of solar-driven rates by *Crovisier et al.* [2006] (solid line) in the atmosphere of Venus. Calculations using the formulation of *Pavlov* [1998] are shown for the day (dot-long-dashed curve) and night (dot-short-dashed curve) atmospheric models of *Gronoff et al.* [2008]. Statistical-equilibrium calculations are shown for an emulation of the night model (crosses), the full model including quenching, radiative cascade and auroral excitation (pluses), the photoelectron spectrum of *Gérard et al.* [2008] at 250 km (solid square) and the auroral spectrum of Gérard et al. at 139 km (bullet).

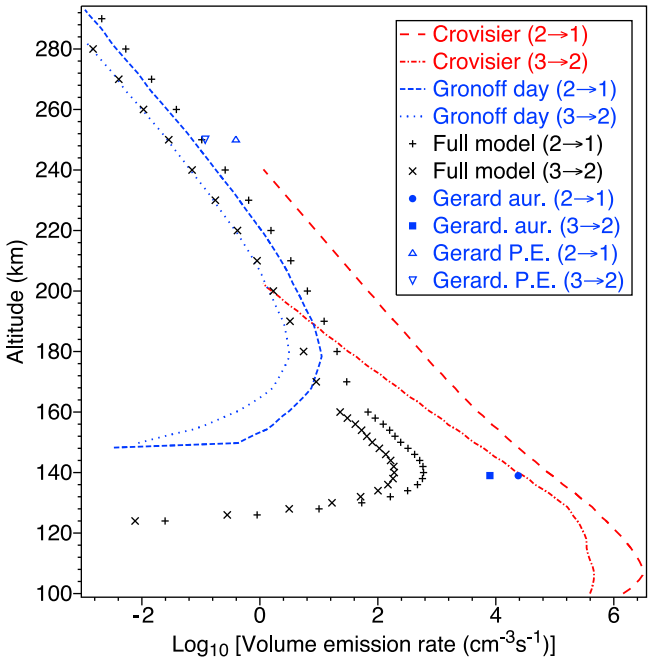

Figure 9. Comparison of electron-driven CO (2 → 1) and (3 → 2) volume emission rates to calculations by *Crovisier et al.* [2006] (long dashed and dot-dashed curves, respectively) in the atmosphere of Venus. Calculations using the formulation of *Pavlov* [1998] are shown for the daytime atmospheric model of *Gronoff et al.* [2008] for (2 → 1) (short dashed curve) and (3 → 2) (dotted curve). Symbols show the statistical-equilibrium calculation for the full model (pluses and crosses), the auroral spectrum of *Gérard et al.* [2008] at 139 km (bullet and solid square) and the photoelectron spectrum of *Gérard et al.* [2008] at 250 km (triangles and inverted triangles).

emission rates using the atmospheric parameters of *Gronoff et al.* [2008] for night and day. The statistical-equilibrium calculation was run to emulate the Gronoff et al. nighttime case, with the agreement confirming that the two implementations are consistent. It was then run for the "Full model", including stepwise decay of the higher vibrational levels of CO, quenching, input from decay of the excited electronic states, and the auroral contribution. The only significant difference is the large increase below about 148 km due to auroral electrons. Emissions calculated using the auroral spectrum of *Gérard et al.* [2008] at 139 km and a photoelectron spectrum of Gérard et al. at 250 km are also shown. All calculated emissions, for both day and night, are substantially less than the daytime emissions of *Crovisier et al.* [2006].

[27] The analysis of Figure 8 is repeated in Figure 9 for daytime CO (2 → 1) and (3 → 2) emissions in the atmosphere of Venus. Impact by thermal electrons is significant (compared to fluorescence and photolysis) above ~190 km for (3 → 2) emissions. The full model shows the auroral contribution is significant below 180 km but predicts emissions that are much less than the solar production. The auroral emissions at 139 km based on the spectrum of *Gérard et al.* [2008] are larger but still much less than the solar-driven emissions. However, using the photoelectron flux spectrum of *Gérard et al.* [2008] gives (2 → 1) emissions at 250 km that are similar to the solar-driven (2 → 1) emissions, while the (3 → 2) emissions are much greater than either solar-driven or thermal-electron (3 → 2) emissions.

5. Conclusions

[28] Using recently measured electron-impact excitation cross sections for the vibrational levels of the ground state of CO and for the $A\ ^1\Pi$ electronic state, together with a statistical-equilibrium method of calculation that allows many processes to be incorporated, volume emission rates of the fundamental vibrational emissions of CO have been determined for the daytime and nighttime atmospheres of Mars and Venus. The electron cooling rates using two different sets of cross sections are similar for both planets, with two exceptions. First, overall the (1 → 0) emissions are higher using the cross sections of *Allan* [2010] as these are larger in magnitude than those of *Poparić et al.* [2006] around the peak at ~1.9 eV. Second, as the measurements of Allan are generally of higher magnitude at electron energies below 1 eV, the emissions calculated using Allan's cross sections are substantially higher for regions where electron temperatures are low. Calculations for the daytime atmosphere of Mars show that (1 → 0) emissions due to impact by thermal electrons are similar to those due to solar excitation above ~180 km, and that the ratio of (2 → 1)/(1 → 0) is substantially different. This indicates that it should be experimentally possible to distinguish between the solar and electron-driven emissions. Emissions due to photoelectrons at 135 km are about 10% of the sunlight-driven production, hence impact by photoelectrons is not significant at this altitude. Auroral emissions are similarly not significant in daytime, but were shown to be significant at night. Calculations of emissions due to thermal electrons at night range from negligible compared to other processes, to much higher, depending on the electron temperature, which is not currently known. Calculations of (1 → 0) emissions in the atmosphere of Venus due to thermal, auroral and photoelectrons are significantly less than emissions from fluorescence and photolysis. However, the (3 → 2) emissions due to thermal electrons become significant above ~190 km while (2 → 1) emissions due to photoelectron impact are similar to the other sunlight-driven emissions at 250 km. Measurements and other calculations for nighttime CO emissions at Venus do not seem to be available, so the volume emission rates presented should be useful in the planning of nighttime measurements.

[29] **Acknowledgments.** This work was supported by the Australian Research Council through its Centres of Excellence Program. M. A. acknowledges Project 200020-113599/1 of the Swiss National Science Foundation. One of us (M.J.B.) thanks the University of Malaya for his "Distinguished Visiting Professor" appointment.

[30] Masaki Fujimoto thanks the reviewers for their assistance in evaluating this paper.

References

Ajello, J. M. (1971), Emission cross sections of CO by electron impact in the interval 1260–5000 Å. I, *J. Chem. Phys.*, *55*, 3158–3168.

Allan, M. (1989), Study of triplet states and short-lived negative ions by means of electron impact spectroscopy, *J. Electron. Spectrosc. Relat. Phenom.*, *48*, 219–351.

Allan, M. (2010), Electron collisions with CO: Elastic and vibrational excitation cross sections, *Phys. Rev. A*, *81*, 042706, doi:10.1103/PhysRevA.81.042706.

Baines, K. H., P. Drossart, M. A. Lopez-Valverde, S. K. Atreya, C. Sotin, T. W. Momary, R. H. Brown, B. J. Buratti, R. N. Clark, and P. D. Nicholson (2006), On the discovery of CO nighttime emissions on Titan by Cassini/VIMS: Derived stratospheric abundances and geological implications, *Planet. Space Sci.*, *54*, 1552–1562.

Beegle, L. W., J. M. Ajello, G. K. James, D. Dziczek, and M. Alvarez (1999), High resolution emission spectroscopy of the A $^1\Pi$ − X $^1\Sigma^+$ fourth positive band system of CO excited by electron impact, *Astron. Astrophys.*, *347*, 375–390.

Billebaud, F., J. Crovisier, E. Lellouch, T. Encrenaz, and J. P. Maillard (1991), High-resolution infrared spectrum of CO on Mars: Evidence for emission lines, *Planet. Space Sci.*, *39*, 213–218.

Brooke, T. Y., G. S. Orton, D. Crisp, A. J. Friedson, and G. L. Bjoraker (1996), Near-infrared spectroscopy of the Shoemaker–Levy 9 impact sites with UKIRT: CO emission from the L site and additional 5-μm spectra, *Icarus*, *121*, 422–430.

Brunger, M. J., S. J. Buckman, and M. T. Elford (2003), Integral cross sections for electron impact excitation of molecules, in *Electron Collisions With Molecules: Scattering and Excitation, Landolt-Börnstein*, vol. I/17C, edited by Y. Itikawa, pp. 6-517–6-518, Springer, New York.

Campbell, L., and M. J. Brunger (2008), Electron cooling by carbon monoxide in the atmospheres of Mars and Venus, *PMC Phys. B*, *1*, 3, doi:10.1186/1754-0429-1-3.

Campbell, L., D. C. Cartwright, M. J. Brunger, and P. J. O. Teubner (2006), Role of electronic excited N_2 in vibrational excitation of the N_2 ground state at high latitudes, *J. Geophys. Res.*, *111*, A09317, doi:10.1029/2005JA011292.

Campbell, L., D. C. Cartwright, and M. J. Brunger (2007), Role of excited N_2 in the production of nitric oxide, *J. Geophys. Res.*, *112*, A08303, doi:10.1029/2007JA012337.

Campbell, L., M. J. Brunger, and T. N. Rescigno (2008), Carbon dioxide electron cooling rates in the atmospheres of Mars and Venus, *J. Geophys. Res.*, *113*, E08008, doi:10.1029/2008JE003099.

Campbell, L., H. Kato, M. J. Brunger, and M. D. Bradshaw (2010), Electron-impact excitation heating rates in the atmosphere of Titan, *J. Geophys. Res.*, *115*, A09320, doi:10.1029/2010JA015482.

Cartwright, D. C., M. J. Brunger, L. Campbell, B. Mojarrabi, and P. J. O. Teubner (2000), Nitric oxide excited under auroral conditions: Excited state densities and band emissions, *J. Geophys. Res.*, *105*, 20,857–20,867, doi:10.1029/1999JA000333.

Choi, Y. W., J. Kim, K. W. Min, A. F. Nagy, and K. I. Oyama (1998), Effect of the magnetic field on the energetics of Mars ionosphere, *Geophys. Res. Lett.*, *25*, 2753–2756.

Crovisier, J., E. Lellouch, C. de Bergh, J.-P. Maillard, B. L. Lutz, and B. Bézard (2006), Carbon monoxide emissions at 4.7 μm from Venus' atmosphere, *Planet. Space Sci.*, *54*, 1398–1414.

Encrenaz, T., E. Lellouch, P. Drossart, H. Feuchtgruber, G. S. Orton, and S. K. Atreya (2004), First detection of CO in Uranus, *Astron. Astrophys.*, *413*, L5–L9.

Fletcher, L. N., P. Drossart, M. Burgdorf, G. S. Orton, and T. Encrenaz (2010), Neptune's atmospheric composition from AKARI infrared spectroscopy, *Astron. Astrophys.*, *514*, A17.

Furlong, J. M., and W. R. Newell (1996), Total cross section measurement for the metastable a $^3\Pi$ state in CO, *J. Phys. B At. Mol. Opt. Phys.*, *29*, 331–338.

Gérard, J.-C., B. Huber, V. I. Shematovich, D. V. Bisikalo, and G. R. Gladstone (2008), The Venus ultraviolet oxygen dayglow and aurora: Model comparison with observations, *Planet. Space Sci.*, *56*, 542–552.

Gibson, J. C., L. A. Morgan, R. J. Gulley, M. J. Brunger, C. T. Bundschu, and S. J. Buckman (1996), Low energy electron scattering from CO: Absolute cross section measurements and R-matrix calculations, *J. Phys. B At. Mol. Opt. Phys*, *29*, 3197–3214.

Gilli, G., M. A. López-Valverde, B. Funke, M. López-Puertas, P. Drossart, G. Piccioni, and V. Formisano (2011), Non-LTE CO limb emission 4.7 μm in the upper atmosphere of Venus, Mars and Earth: Observations and modeling, *Planet. Space Sci.*, *59*, 1010–1018, doi:10.1016/j.pss.2010.07.023.

González-Galindo, F., M. A. López-Valverde, M. Angelats i Coll, and F. Forget (2005), Extension of a Martian general circulation model to thermospheric altitudes: UV heating and photochemical models, *J. Geophys. Res.*, *110*, E09008, doi:10.1029/2004JE002312.

Gronoff, G., J. Lilensten, C. Simon, M. Barthélemy, F. Leblanc, and O. Dutuit (2008), Modelling the Venusian airglow, *Astron. Astrophys.*, *482*, 1015–1029.

Kasprzak, W. T., H. B. Niemann, A. E. Hedin, S. W. Bougher, and D. M. Hunten (1993), Neutral composition measurements by the Pioneer Venus neutral mass spectrometer during orbiter re-entry, *Geophys. Res. Lett.*, *20*, 2747–2750.

Kato, H., H. Kawahara, M. Hoshino, H. Tanaka, M. J. Brunger, and Y.-K. Kim (2007), Cross sections for electron impact excitation of the vibrationally resolved *A* $^1\Pi$ electronic state of carbon monoxide, *J. Chem. Phys.*, *126*, 064307.

Lawrence, G. M. (1971), Quenching and radiation rates of CO (a $^3\Pi$), *Chem. Phys. Lett.*, *9*, 575–577.

Leblanc, F., O. Witasse, J. Winningham, D. Brain, J. Lilensten, P.-L. Blelly, R. A. Frahm, J. S. Halekas, and J. L. Bertaux (2006), Origins of the Martian aurora observed by spectroscopy for investigation of characteristics of the atmosphere of Mars (SPICAM) on board Mars Express, *J. Geophys. Res.*, *111*, A09313, doi:10.1029/2006JA011763.

Lillis, R. J., M. O. Fillingim, L. M. Peticolas, D. A. Brain, R. P. Lin, and S. W. Bougher (2009), Nightside ionosphere of Mars: Modeling the effects of crustal magnetic fields and electron pitch angle distributions on electron impact ionization, *J. Geophys. Res.*, *114*, E11009, doi:10.1029/2009JE003379.

López-Valverde, M. A., and M. López-Puertas (1994), A non-local thermodynamic equilibrium radiative transfer model for infrared emissions in the atmosphere of Mars: 1. Theoretical basis and nighttime populations, *J. Geophys. Res.*, *99*, 13,093–13,115.

Morrison, M. A., and A. E. Greene (1978), Electron cooling by excitation of carbon dioxide, *J Geophys Res*, *83*, 1172–1174.

Nagy, A. F., and T. E. Cravens (2002), Solar system ionospheres, in *Atmospheres in the Solar System: Comparative Aeronomy*, *Geophys. Monogr. Ser.*, vol. 130, edited by M. Mendillo, A. Nagy, and J. H. Waite, pp. 39–52, AGU, Washington, D. C.

Nier, A. O., and M. B. McElroy (1977), Composition and structure of Mars' upper atmosphere: Results from the neutral mass spectrometers on Viking 1 and 2, *J. Geophys. Res.*, *82*, 4341–4349.

Pavlov, A. V. (1998), New electron energy transfer rates for vibrational excitation of N_2, *Ann Geophys.*, *16*, 176–182.

Poparić, G. B., D. S. Belić, and M. D. Vićić (2006), Resonant vibrational excitation of CO by low-energy electrons, *Phys. Rev. A*, *73*, 062713.

Shematovich, V. I., D. V. Bisikalo, J.-C. Gérard, C. Cox, S. W. Bougher, and F. Leblanc (2008), Monte Carlo model of electron transport for the calculation of Mars dayglow emissions, *J. Geophys. Res.*, *113*, E02011, doi:10.1029/2007JE002938.

Slanger, T. G., T. E. Cravens, J. Crovisier, S. Miller, and D. F. Strobel (2008), Photoemission phenomena in the solar system, *Space Sci. Rev.*, *139*, 267–310, doi:10.1007/s11214-008-9387-3.

Spenner, K., W. C. Knudsen, and W. Lotze (1996), Suprathermal electron fluxes in the Venus nightside ionosphere at moderate and high solar activity, *J. Geophys. Res.*, *101*, 4557–4563.

Starr, D. F., and J. K. Hancock (1975), Vibrational energy transfer in CO_2–CO mixtures from 164 to 406°K, *J. Chem. Phys.*, *63*, 4730–4734.

M. Allan, Department of Chemistry, University of Fribourg, chemin du Musée 9, CH-1700 Fribourg, Switzerland.

M. J. Brunger and L. Campbell, ARC Centre for Antimatter-Matter Studies, School of Chemical and Physical Sciences, Flinders University, GPO Box 2100, Adelaide, SA 5001, Australia. (laurence.campbell@flinders.edu.au)